Please cite the Published Version

Additional Information: This is an open access article which first appeared in Electroanalysis

Data Access Statement: The data that support the findings of this study are available from the corresponding author upon reasonable request.

RESEARCH ARTICLE OPEN ACCESS

Additive Manufacturing Electrochemistry: Development of Bismuth Oxide Microparticle Filament for Lead (II) Detection

Enyioma C. Okpara[1,2] | Robert D. Crapnell[2] | Elena Bernalte[2] | Olanrewaju B. Wojuola[1] | Craig E. Banks[2] (ORCID)

[1]Department of Physics, Faculty of Natural and Agricultural Science, North-West University (Mafikeng Campus), Private Bag, X2046, Mmabatho, South Africa | [2]Faculty of Science and Engineering, Manchester Metropolitan University, Dalton building, Manchester, Great Britain

Correspondence: Craig E. Banks (c.banks@mmu.ac.uk)

ABSTRACT

Accurate, rapid, and cost-effective validation of water quality is essential to ensure that the World Health Organization's (WHO) standards are met and that the United Nations Sustainable Development Goal 6—Clean Water and Sanitation is achieved. To this end, the development of additive-manufactured electrodes using recycled polylactic acid, nanocarbon black, and micro-sized bismuth oxide is reported. These electrodes, that are fabricated using a thermal mixing approach, can be customized to incorporate varying amounts of bismuth oxide (1, 2.5, and 5 wt%) maintaining the integrity of the base polymer. The electrodes developed in this work demonstrate significant potential for the electrochemical detection of lead (II) within water, achieving limits of detection of 0.79, 0.93, and 4.29 $\mu g\,L^{-1}$ (3σ), for the 1, 2.5, and 5 wt% bismuth oxide sensors, respectively. These detection limits are notably below the WHO recommended threshold of 10 $\mu g\,L^{-1}$ for lead in domestic water and even achieve the 2036 European Union targets of 5 $\mu g\,L^{-1}$. The 2.5 wt% bismuth oxide electrodes exhibit excellent reproducibility and specificity, achieving average recovery rates of 98.28% and 100.15% in the analysis of spiked lead (II) samples in deionized and condensed atmospheric water, respectively. This approach is further validated against inductively coupled plasma mass spectroscopy measurements.

1 | Introduction

Lead is a common toxic metal with no safe level and it has widespread use globally. The Institute for Health Metrics and Evaluation (IHME) reports that lead exposure accounts for more than 33 million years lost to disability, globally [1]. Lead poisoning can occur upon entry to the body through contaminated water, air, dust, food, or consumer products and can cause problems in the bones, teeth, blood, liver, kidneys, and brain [2]. Both acute and chronic lead exposure at any level has the potential to be harmful. Elevated blood lead levels in children have been linked to neurological effects such as behavioral and learning problems, hearing problems, hyperactivity, lower IQ, and impaired development, while in contrast, low lead levels have been linked with irreversible neurocognitive, maladaptive, and behavioral, developmental disorders [2, 3]. Important sources of environmental contamination of lead include manufacturing, mining, smelting, and recycling activities due to its use in a range of products including jewelry, toys, lead crystal glassware, pigments, paints, solder, stained glass, and ceramic glazes. Moreover, lead can contaminate drinking water through plumbing systems containing lead pipes, solders, and fittings. The risk of lead poisoning can be through drinking tap water if your residence (property) has lead pipes, lead water tank, and pipework with lead fittings which can result in lead contaminating the water supply. Therefore, the need to accurately detect trace

---

amounts of this heavy metal ion, among other of similar importance, in drinking water is not just crucial but urgent for effectively measuring water pollution and protect human health. The World Health Organization's (WHO) and US Environmental Protection Agency (EPA) guidelines recommended guideline values for maximum allowable concentration of lead in drinking water, set at $10\,\mu g\,L^{-1}$ [4].

Traditional analytical techniques such as atomic absorption spectroscopy (AAS), inductively coupled plasma mass spectroscopy (ICP-MS), and X-ray fluorescence spectrometry offer certain benefits for detecting heavy metal ions; however, these methods involve expensive equipment, trained personnel, and complex operations. In contrast, electrochemical analysis methods have gained attention due to their high sensitivity, quick analysis, affordability, ease of operation, and convenient field monitoring. Specifically, anodic stripping voltammetry is widely applied for the measurement of lead and provides a cost-effective, rapid, simple to operate, and highly sensitive analytical method for detecting heavy metal ions [5]. Traditionally, mercury-based electrodes were utilized as a beneficial approach for the sensing of lead, but nowadays this is limited by its toxicity. Another alternative approach extensively reported in the literature is the use of bismuth-based electrodes which offers lower toxicity [6]. In this way, the creation of multicomponent alloys can create fusible alloys with various heavy metals, which show well-defined, undistorted and highly reproducible responses, favorable resolution of neighboring peaks with good signal-to-background characteristics comparable to those of common mercury electrodes [6]. This approach has been reported for ex-situ formation [7], in situ formation, [8] and more recently modified screen-printed electrodes [9–12].

One innovative approach to fabricate electrochemical-based sensors is through utilizing additive manufacturing [13]. Additive manufacturing, often called 3D printing, encompasses a group of processes that transform computer-aided design files into physical objects by depositing material in successive thin layers. Among the most widely used and cost-effective methods is fuzed filament fabrication, also known as fuzed deposition modeling. This technique works through the deposition of thermoplastic polymers and is notable for its affordability, with printers available for a few hundred pounds, compared to the thousands or even hundreds of thousands required for other types of printers. Using additive manufacturing to create electrodes involves selecting filaments or materials that meet the electrical, chemical, and mechanical requirements of the application. The choice of filaments depends on the type of electrode (e.g., for batteries, fuel cells, sensors, or supercapacitors) and the additive manufacturing technology being employed. There are commercially available conductive filaments on the market, but these have poor conductivity and stability. Therefore, researchers are developing new filaments allowing them to realize next-generation electrochemical-based sensors with different carbon compounds inducing significantly improved conductivities [13–15]. Researchers are beginning to take this further through the incorporation of nano-materials and metallic modifiers to improve the performance of filament further for specific applications [16, 17].

In this paper, we report additive-manufactured electrodes with the development of recycled polylactic acid, nanocarbon black (CB), and micro-sized bismuth oxide. We show that these can be readily tailored to encompass different amount of bismuth oxide, namely, 1, 2.5, and 5 wt%, which are shown to be beneficial for the sensing of lead (II) in water samples.

2 | Experimental Section

2.1 | Chemicals

All chemicals used in the experiment were of analytical grade and were used as received without any additional purification. The solutions were prepared using deionized water (DIW) with a resistivity of at least $18.2\,M\Omega\,cm$, obtained from a Milli-Q Integral 3 system from Millipore UK (Watford, UK). Hexaammineruthenium (III) chloride (98%), castor oil, sodium hydroxide (>98%), acetic acid (>99%), sodium phosphate dibasic (>99%), lead and copper standards for AAS ($1\,g\,L^{-1}$), micro-sized bismuth oxide (>99%), and potassium chloride (99.0%–100.5%) were purchased from Merck (Gillingham, UK). Nano-CB (>99+%) was purchased from Pi-kem (Tamworth, UK). Recycled poly (lactic acid) (rPLA) was purchased from Gianeco (Turin, Italy).

2.2 | Production of Recycled Filament

This follows our previous work, where we have reported the use of rPLA using castor oil as a bio-based plasticizer and with a conductive element using nano-CB [18]; see Scheme 1 for an overview. In this approach, we manufacture a polymer blend comprising rPLA, castor oil, and nano-CB. All recycled rPLA was dried in an oven at 60°C for at least 2.5 h to eliminate any remaining moisture in the polymer. The polymer composites were mixed in a chamber at 190°C with Banbury rotors at 70 rpm for 5 min using a Thermo Haake Polydrive dynameter equipped with a Thermo Haake Rheomix 600 (Thermo-Haake, Germany). The resulting polymer composite was allowed to cool down to room temperature and then granulated to achieve a finer granule size using a Rapid Granulator 1528 (Rapid, Sweden). The granulated sample was collected and processed through the hopper of the EX2 extrusion line (Filabot, VA, United States) with heat zone set at 195°C. The molten polymer was extruded from a 1.75 mm die head, pulled along an airpath cooling line (Filabot, VA, USA) through an in-line measure (Mitutoyo, Japan), and collected on a Filabot spooler (Filabot, VA, USA). The filaments modified with Bi_2O_3 were prepared in the same way, with 1, 2.5, and 5 wt% Bi_2O_3 added to replace CB, hence producing the following: 1% Bi_2O_3, 55 wt% rPLA, 10 wt% castor oil, and 34 wt% nano-CB; 2% Bi_2O_3, 55 wt% rPLA, 10 wt% castor oil, and 33 wt% nano-CB; 5% Bi_2O_3, 55 wt% rPLA, 10 wt% castor oil, and 30 wt% nano-CB. The filaments are then ready to use for additive manufacturing.

2.3 | Additive Manufacturing

The computer designs and 0.3MF files in this manuscript were created using Fusion 360 by Autodesk. These files were then prepared for additive manufacturing using PrusaSlicer, specific to Prusa Research's printers. A 0.6 mm nozzle was used, with a
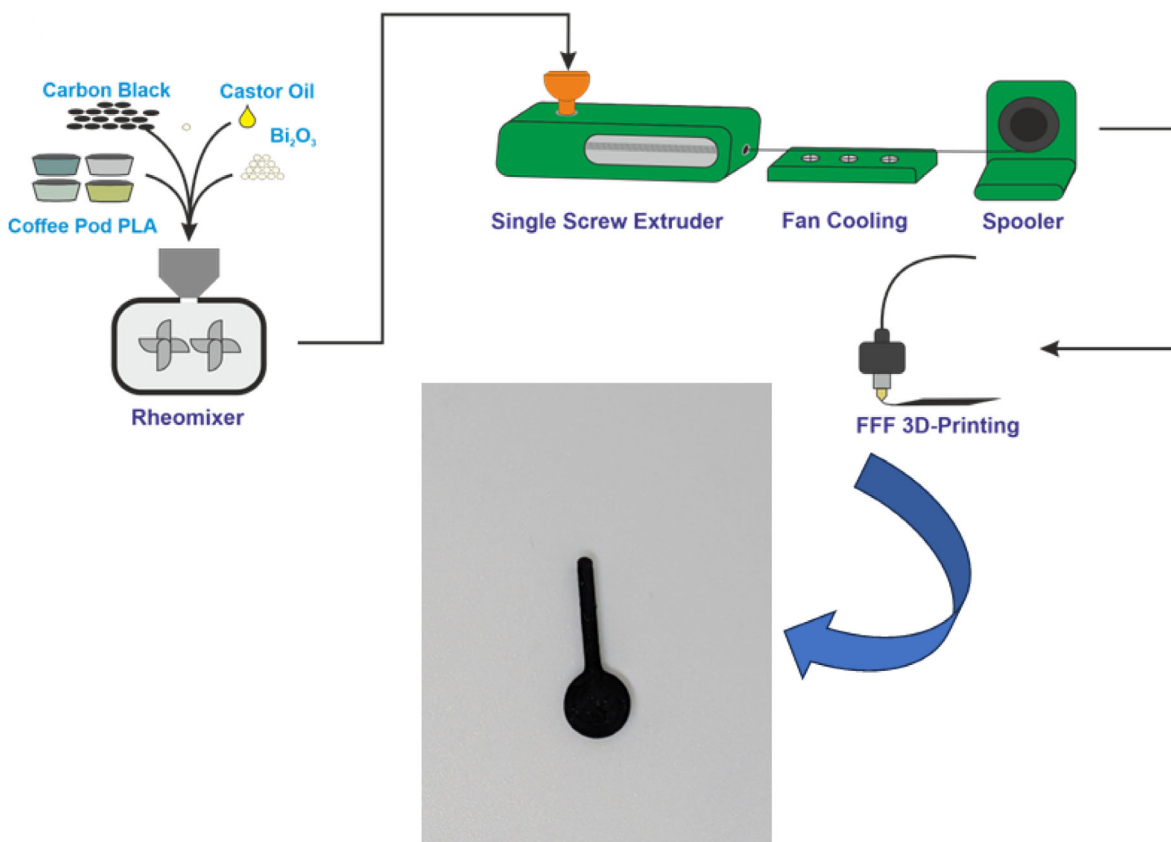
SCHEME 1 | An overview of how the BiO filament is made with the resulting electrode shown (dimensions: Ø 5 mm disc with 8 mm connection length and 2 × 1 mm thickness).

nozzle temperature of 225°C, an extrusion ratio of 1.6 (160%), 100% rectilinear infill [19], a 0.2 mm layer height, and a print speed of 35 mm s^{-1}. The increased extrusion ratio was necessary because the filament's diameter was approximately 1.6 mm, slightly below the de facto 1.75 mm standard used by PrusaSlicer for extrusion calculations. This produced an additive-manufactured lollipop shape with Ø 5 mm disc with 8 mm connection length and 2 × 1 mm thickness.

2.4 | Physicochemical Characterization

X-ray photoelectron spectroscopy (XPS) data were acquired using a Kratos AXIS Supra instrument with a monochromated Al X-ray source operating at 225 W. The instrument was set to fixed transmission mode for survey and region scans. The collimator operated in slot mode for an analysis area of approximately 700 × 300 μm. Scanning electron microscopy (SEM) was carried out using a Carl Zeiss Supra 40VP field-emission instrument with an average chamber and gun vacuum of 1.3×10^{-5} and 1×10^{-9} mbar, respectively. The samples were sputtered with a thin layer of Au/Pd to enhance image contrast.

2.5 | Electrochemical Studies

All electrochemical experiments were performed on an Autolab 100N potentiostat controlled by NOVA 2.1.7 (Utrecht, The Netherlands) and Ivium Compactstat potentiostat controlled by IviumSoft software. Identical additive-manufactured electrodes were used throughout this work for all filaments, printed in a lollipop shape (Ø 5 mm disc with 8 mm connection length and 2 × 1 mm thickness) [20] alongside an external commercial Ag|AgCl/KCl (3M) reference electrode with a Nichrome wire counter electrode. All solutions of $[Ru (NH_3)_6]^{3+}$ were purged of O_2 thoroughly using N_2 prior to any electrochemical experiments. The additive-manufactured electrodes are activated as documented in the literature [15], which use chronoamperometry at a voltage of +1.4 V for 200 s, followed by applying −1.0 V for 200 s within 0.5 M sodium hydroxide. The additive-manufactured electrodes were then thoroughly rinsed with DIW and dried under compressed air before further use.

2.6 | Real Sample Analysis

To acquire atmospheric water for sample analysis, a medium-sized sample bag was filled with DIW and securely sealed to prevent contamination. This sealed bag was placed inside a larger sample bag, ensuring that it did not contact any surfaces. The bag was then frozen overnight to turn the water into ice. The resulting ice was then positioned near a laboratory window close to the experimental workstation for around 6 h, causing it to melt and condensed water to collect in the larger sample bag. This process was repeated twice to obtain almost 200 mL of condensed atmospheric water (CAW) for use in the sample analysis. Two separate solutions were meticulously prepared for analysis using DIW and CAW samples. To ensure accurate measurements, a

supporting electrolyte of 0.1 M acetate buffer solution at pH 4.5 was incorporated into each solution. The electrochemical determination of the lead (II) was carried out by using square-wave anodic stripping voltammetry (SWASV). For this purpose, 10 mL of each water sample was spiked with Pb^{2+}, where the standard addition method is employed.

2.7 | Validation Using ICP-MS Analysis

Water sample analysis for lead was performed using an Agilent 7900 ICP-MS with Agilent integrated autosampler. A six-point calibration series was created by dilution from QMX Multi Element Standard 2a for ICP-MS, spanning $0.1–100~\mu g\,L^{-1}$. The sample sequence was developed with initial rinses, the calibration series, a quality control ($10~\mu g\,L^{-1}$ QC), method blanks, the samples, and a $10~\mu g\,L^{-1}$ QC sample at the end. The calibration line fit for all four elements were better than 0.999, QC samples showed no significant drift across the analysis time.

3 | Results and Discussion

3.1 | Physicochemical Characterization of Bi_2O_3 AdditiveManufactured Electrodes

Initially, additive-manufacturing filaments comprising rPLA and nano-CB and using castor oil as the plasticizer using our previous approach (please see Experimental Section) were fabricated [18].

Of note, we have used castor oil as an inedible oil that can be extracted through solvent or mechanical pressing from the plant *Ricinus communis* (*Euphorbiaceous* family). This is a bio-based plasticizer helping, in part, to transition to the sustainable production of filament [18]. In this work, we created filament with 10 wt% higher loading of nano-CB when compared to previous reports. This highlights the excellent plasticizing performance of the castor oil. Alongside this, filament containing bismuth oxide (Bi_2O_3) added to replace CB was fabricated in the following compositions: 1 wt% Bi_2O_3, 55 wt% rPLA, 10 wt% castor oil, and 34 wt% nano-CB; 2.5 wt% Bi_2O_3, 55 wt% rPLA, 10 wt% castor oil, and 33 wt% nano-CB; 5 wt% Bi_2O_3, 55 wt% rPLA, 10 wt% castor oil, and 30 wt% nano-CB. We term these simply as 1%, 2.5% and 5% Bi_2O_3 additive-manufactured electrodes. We explore the additive-manufactured electrode with SEM and XPS. As shown within Figure 1A, the SEM is shown of the surface of a 2.5% Bi_2O_3 additive-manufactured electrodes and also, the EDX, as illustrated in Figure S1. These effectively demonstrate the presence of bismuth oxide in the additive-manufactured electrode, where one can observe the presence of carbon, oxygen, and bismuth. The chemical composition of the additive-manufactured electrodes are investigated through XPS; the spectra of the additive-manufactured electrode are shown in Figure 1B–D. Figure 1B shows the full spectra scan where part C and D shows the C 1s (Figure 1C) and Bi 4f regions (Figure 1D).

The analysis of the C 1s spectra (Figure 1C) indicates the presence of the following moieties where three smaller symmetric peaks are assigned to O—C=O, C=O, and C—O, while a fourth
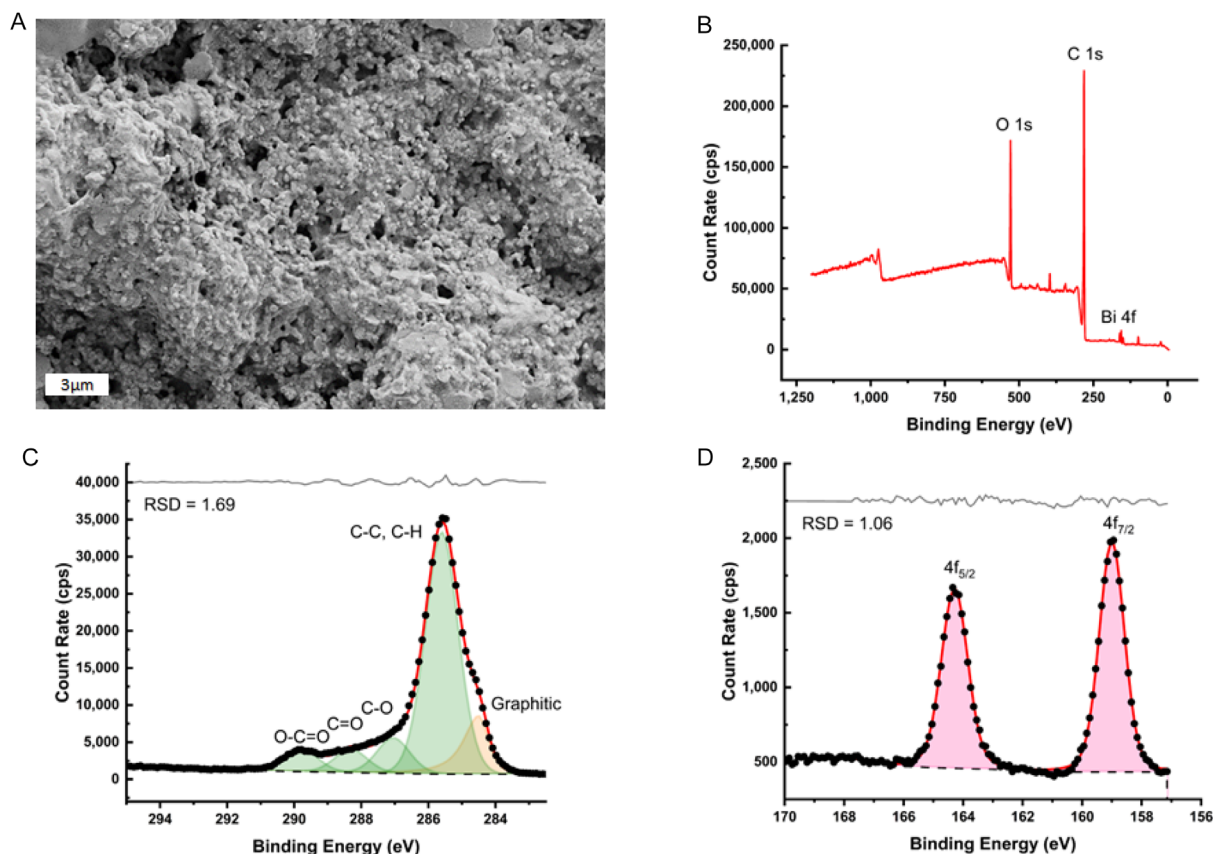
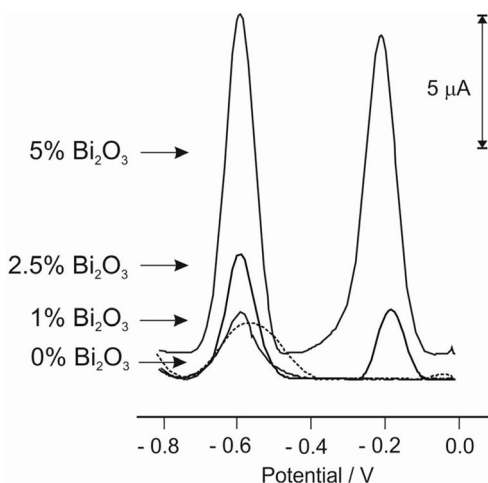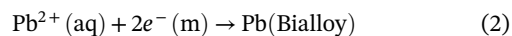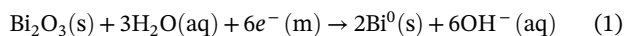**FIGURE 1** | The SEM images of (A) the 2.5% Bi_2O_3 additive-manufactured electrode. XPS survey spectra of (B) the additive-manufactured electrode with the regions shown are (C) C 1s and (D) Bi 4f. SEM = scanning electron microscope; XPS = X-ray photoelectron spectroscopy.

larger symmetric peak is assigned to C—C and C—H bonding. There was also the requirement for fitting an asymmetric peak at 284.5 eV, which corresponds to the X-ray photoelectron emission from graphitic carbon [21]. Two symmetrical peaks are shown in Figure 1D, corresponding to the bismuth $4f_{7/2}$ and $f4_{5/2}$, with peaks located at 159.0 and 164.3 eV, respectively. This shows agreement with the well-defined separation of Bi 4f spin–orbit components of 5.3 eV [22].

## 3.2 | Electrochemical Characterization and SWASV Optimization

The 2.5% Bi_2O_3 additive-manufactured electrode was benchmarked using an outer sphere probe, using $[Ru(NH_3)_6]^{3+}$ (1 mM in 0.1 M KCl), which produced a heterogeneous rate constant, k^0, of $1.61 \pm 0.45 \times 10^{-3}$ cm s^{-1}. In comparison, the commercial additive-manufactured electrodes using Protopasta (only containing CB) had a k^0 value of $0.30\,(\pm 0.03) \times 10^{-3}$ cm s^{-1} [18], demonstrating the enhanced performance of this filament in fabricating additive-manufactured electrodes. Through the use of the *quasi*-reversible Randles–Ševčík equation, the real electrochemical surface area (A_e) is determined to be 0.76 (± 0.07) cm^2.

Next, we explore the use of 0%, 1%, 2.5%, and 5% Bi_2O_3 additive-manufactured electrodes toward the sensing of lead (II). Note that this approach avoids the need for ex-situ bismuth film plating or in-situ bismuth film formation via the addition of bismuth salts. As shown within Figure 2, bismuth oxide is electrochemically reduced forming bismuth metal when a sufficiently negative potential is held and in the presence of lead undergoes the following transformation [9, 23]:

$$Bi_2O_3(s) + 3H_2O(aq) + 6e^-(m) \rightarrow 2Bi^0(s) + 6OH^-(aq) \quad (1)$$

$$Pb^{2+}(aq) + 2e^-(m) \rightarrow Pb(Bialloy) \quad (2)$$

FIGURE 2 | SWASV (-1.1 V deposition potential; 120 s deposition time at 800 rpm) of 30 µg L^{-1} of lead (II) in 0.1 M acetate buffer recorded using 0% Bi_2O_3 (dotted line) alongside 1%, 2.5%, and 5% Bi_2O_3 additive-manufactured electrodes. All potentials are against Ag/AgCl. SWASV = square-wave anodic stripping voltammetry.

On the anodic sweep, two peaks are observed which correspond to

$$2Bi^0(s) \rightarrow Bi^{3+}(aq) + 3e^- \quad (3)$$

$$Pb(Bi\ alloy) \rightarrow Pb^{2+}(aq) + 2e^-(m) \quad (4)$$
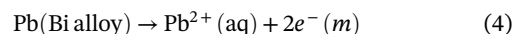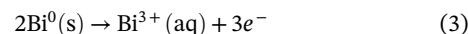
Using a 1% Bi_2O_3 additive-manufactured electrode does not show a stripping peak from bismuth due to the low amount contained within the electrode surface but it is readily seen when a 2.5% Bi_2O_3 additive-manufactured electrodes is used. One can readily see that the use of bismuth oxide results in a sharp peak where the nucleation kinetics is favorable against that of the bare additive-manufactured electrodes. To detect lead (II) using SWASV, we explored the optimal deposition potential and time. During the study, other instrumental parameters, such as the step potential, amplitude, and frequency, were held constant: amplitude of 60 mV, potential step of 4 mV, and a frequency of 10 Hz. This allowed for a comprehensive and controlled analysis of the detection process. The impact of deposition time (ranging from 60 to 180 s due to stirring) on the lead (II) voltammetric responses was initially investigated employing 80 µg L^{-1} of lead (II) analyte in 0.1 M acetate buffer using a 2.5% Bi_2O_3 additive-manufactured electrode. As anticipated, the peak
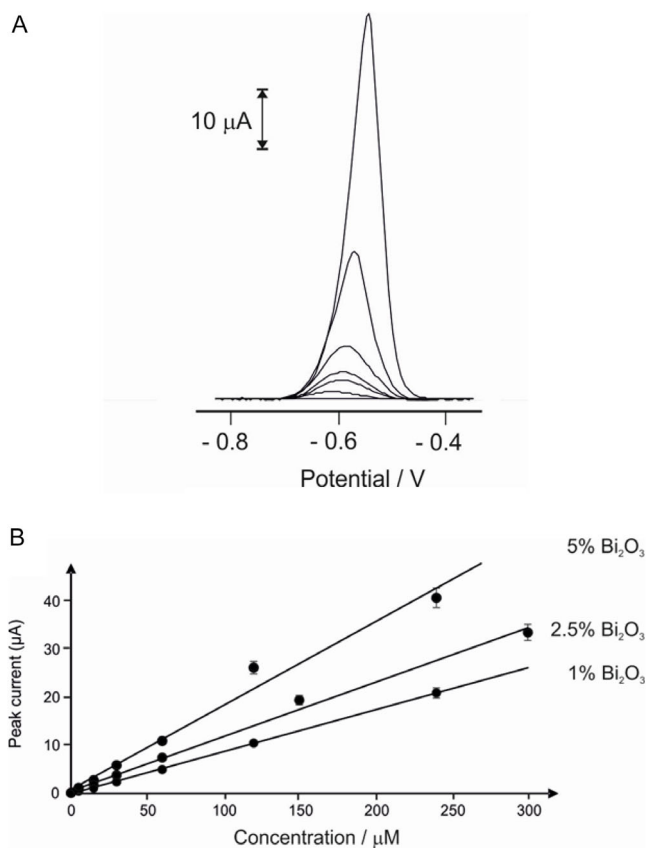
FIGURE 3 | (A) Optimized SWASV for the increasing concentration of lead (II) (0.1 M acetate buffer) using 2.5% Bi_2O_3 additive-manufactured electrode. (B) Calibration curves for the response of the peak height against increasing concentrations of lead (II) (0.1 M acetate buffer) for the 1%, 2.5% and 5% Bi_2O_3 additive-manufactured electrodes. An average of three measurements are shown where the standard deviation is represented. SWASV = square-wave anodic stripping voltammetry.

currents exhibited a consistent increase with longer accumulation times of up to 120 s, followed by a sharp and steady decline. This observed pattern aligns with previous findings, traditionally associated with the saturation of the electroactive area of the electrode [24]. Maintaining the accumulation time at 120 s, we proceeded to examine the influence of the deposition potential, which varied from −1.2 to −0.8 V, where the highest current response was observed at −1.1 V. Consequently, the optimal values for the deposition potential and time were determined based on the maximum current values at −1.1 V and 120 s, respectively, and were selected for further experiments.

Attention is turned to explore the sensing of lead (II) using the 1%, 2.5%, and 5% Bi_2O_3 additive-manufactured electrodes, as shown in Figure 3A, where it can be seen that typical SWASV for the increasing concentration of lead (II) using the 2.5% Bi_2O_3 additive-manufactured electrodes, where also shown are the calibration curves for the response of the peak height against increasing concentrations of lead (II) 0−300 µg L^{-1} for the 1%, 2.5%, and 5% Bi_2O_3 additive-manufactured electrodes; further lead (II) additions resulted in deviation. Regression equations are as follows: 1% Bi_2O_3: I_p/µA = 0.0876 µg L^{-1} − 0.0532, $R^2 = 0.9997$; 2.5% Bi_2O_3: I_p/µA = 0.1451 µg L^{-1} − 0.2313, $R^2 = 0.9996$; and 5% Bi_2O_3: y I_p/µA = 0.1884 µg L^{-1} + 0.037, $R^2 = 0.9930$. Interestingly, more comprehensive concentration range of 0−300 µg L^{-1} was achieved which is taken forward to the real sample analysis. A summary of the sensor is compared to other reports. These values nonetheless fall far below the limits set by the WHO [25], which is 10 µg L^{-1}, and are comparable to results found in existing literature (see Table 1), where one can

TABLE 1 | Comparison of additive-manufactured electrodes for the sensing of lead (II) with literature reports.

Electrode composition	Technique	Linear range	Limit ofdetection	Sample medium	Reference
Bi film SPE/Nafion	SWASV	20–300 µg L^{-1}	3 µg L^{-1}	River and tap water	[26]
Bi film SPE	SWASV	20–100 µg L^{-1}	2.3 µg L^{-1}	River water	[27]
AME: PLA/nano-sized Bi/PGE	DPASV	10–100 µg L^{-1}	0.39 µg L^{-1}	Bottled water	[17]
AME: PLA/CB/micro-sized Bi_2O_3	DPASV	5–60 µg L^{-1}	0.45 µg L^{-1}	Bottled water	[28]
Bi_2O_3/bulk SPE	SWASV	5–150 µg L^{-1}	5.00 µg L^{-1}	—	[29]
AME: 1% Bi_2O_3, 55 wt% rPLA, 10 wt% CO, 34 wt% CB	SWASV	0–240 µg L^{-1}	0.79 µg L^{-1}	—	This work
AME: 2.5% Bi_2O_3, 55 wt% rPLA, 10 wt% CO, and 33 wt% CB	SWASV	0–300 µg L^{-1}	0.93 µg L^{-1}	DIW; CAW	This work
AME: 5% Bi_2O_3, 55 wt% rPLA, 10 wt% CO, and 30 wt% CB	SWASV	0–120 µg L^{-1}	4.29 µg L^{-1}	—	This work

Abbreviations: AME: additive-manufactured electrodes; CAW: condensed atmospheric water; CB: carbon black; CO: castor oil; DIW: deionized water; DPASV: differential pulse anodic stripping voltammetry; PGE: polyethylene glycol dimethyl ether; SPE: screen-printed electrode; and SWASV: square-wave anodic stripping voltammetry.

TABLE 2 | Investigation of lead (II) within spiked deionized water (DIW) and condensed atmospheric water (CAW) samples.

DIW Sample (Pb^{2+})	Spiked (µg L^{-1})	Detected (µg L^{-1})	Recovery (%)	RSD (%)
1	15	14.94	99.63	14.53
2	30	28.05	93.50	3.47
3	60	60.97	101.62	9.83
Average			98.28	9.28
CAW sample (Pb^{2+})	Spiked (µg L^{-1})	Detected (µg L^{-1})	Recovery (%)	RSD (%)
1	15	15.79	105.23	19.33
2	30	28.21	94.05	9.72
3	60	60.70	101.17	13.45
Average			100.15	14.16
Technique	SWASV	ICP-MS[a]	SWASV[a]	ICP-MS	% Contrast
DIW	BDL	0.05	14.94 ± 2.08	16.55	10.78
CAW	BDL	0.04	15.79 ± 2.46	13.21	16.34

Abbreviations: BDL: below detection limit; CAW: condensed atmospheric water; DAW: deionized water; ICP-MS: inductively coupled plasma mass spectroscopy; SWASV: square-wave anodic stripping voltammetry.
[a]15 ppb of Pb^{2+} spiked in each sample. The standard deviation is the result of three electrode-to-electrode repetitive runs using the proposed technique taken at a 95% confidence level. Relative standard deviation (RSD).

observe that our additive manufacturing electrochemical system provides competitive outputs.

3.3 | Interference Studies and Electroanalytical Application for Lead (II) Detection

Prior studies have indicated that the presence of nontarget Cu^{2+} can interfere with the accurate determination of Pb^{2+} in bismuth-based electrodes [10, 30], while other nontarget ions such as K^+, Na^+, Ca^{2+}, Cl^-, NO_3^-, and Fe^{3+} may not have the same effect [31]. We explored the impact of varying concentrations of 50–1000 $\mu g\,L^{-1}$ copper (II) using 2.5% Bi_2O_3 additive-manufactured electrodes for the sensing of 30 $\mu g\,L^{-1}$. In the presence of 50 $\mu g\,L^{-1}$ of copper (II), the electrode sensitivity decreased by only 8.53% ($n = 3$) but in the presence of 1000 $\mu g\,L^{-1}$ Cu^{2+} the electrode sensitivity was reduced by 63%, leading to a substantial decrease in the average recovery rate. See Figure S2 which shows the effect on the sensing of lead (II) in the presence of 10 and 1000 $\mu g\,L^{-1}$ copper (II). Wang et al. [32]. have attributed this to the competition between electrodeposited bismuth and copper for surface sites on the electrode, as well as the formation of intermetallic compounds between copper and lead. Therefore, it is important to pretreat water samples containing high concentrations of copper (II) before conducting measurements [11].

Last, we turn to the measurement of lead (II) with real samples. A 10 mL sample of DIW and CAW was used for real sample analysis using 2.5% Bi_2O_3 additive-manufactured electrodes. Both water samples were spiked with a 5 $\mu g\,L^{-1}$ standard solution, resulting in a noticeable stripping peak for Pb^{2+}. By using the standard addition method, a final solution of 60 $\mu g\,L^{-1}$ was achieved in both water samples to determine the concentration of Pb^{2+}. The results are specified in Table 2, where the spiked Pb^{2+} recoveries in the water samples ranged from 93.50% to 101.1% (average 98.25 ± 4.23)% in DIW and from 94.05% to 105.23% (average 100.15 ± 5.66)% in CAW. In a validation study, the analytical efficacy of the engineered 2.5% Bi_2O_3 additive-manufactured electrodes was ascertained through standard ICP-MS analysis. The ICP-MS detected Pb^{2+} concentrations in acidified (2% v/v nitric acid) DIW and condensed water samples at 0.05 and 0.04 $\mu g\,L^{-1}$, respectively, values that fall below the detection thresholds of the developed methodology and instrumentation. Subsequently, these samples were enriched with a 15 $\mu g\,L^{-1}$ Pb^{2+} standard solution and subjected to analysis using the proposed approach (Table 2). The additive-manufactured sensor are demonstrated to provide an analyte concentration that was comparable to the ICP-MS value, with a better recovery rate compared to the ICP-MS. In summary, we show that the use of 2.5% Bi_2O_3 additive-manufactured sensor is accurate and precise in determining Pb^{2+} in DIW and CAW samples.

4 | Conclusions

In summary, we have engineered additive-manufactured electrodes with the development of recycled polylactic acid, nano-CB, and micro-sized bismuth oxide. We show that these can be readily tailored to encompass different amount of bismuth oxide (1, 2.5, and 5 wt%) and are beneficial for the sensing of lead (II). Using 1, 2.5, and 5 wt% bismuth oxide additive-manufactured electrodes, we show that limits of detection of 0.79, 0.93, and 4.29 $\mu g\,L^{-1}$ (3σ) are feasible. Such an approach removes the need for ex-situ bismuth plating or in-situ bismuth film formation via the addition of bismuth salts. The detected limits are significantly lower than the WHO recommended guideline values for domestic water, set at 10 $\mu g\,L^{-1}$. The 2.5% bismuth oxide additive-manufactured electrodes show a good level of reproducibility and specificity, with an average recovery rate of 98.28% and 100.15% in the analysis of spiked lead (II) DIW and CAW samples, respectively, and our approach is validated against ICP-MS.

Conflicts of Interest

The authors declare no conflicts of interest.

Data Availability Statement

The data that support the findings of this study are available from the corresponding author upon reasonable request.

References

1. https://www.who.int/news-room/fact-sheets/detail/lead-poisoning-and-health.https://www.healthdata.org/research-analysis/diseases-injuries-risks/factsheets/2021-lead-exposure-level-3-risk.

2. Z. Wen, D. Zheng, J. Wu, et al., "Integral Trends in Research of Lead Exposure and Child Health from 2012 to 2022: A Bibliometric Analysis," *Environmental Science and Pollution Research* 31, no. 6 (2024): 9251–9271, https://doi.org/10.1007/s11356-023-31744-6.

3. D. Ramírez Ortega, D. F. González Esquivel, T. Blanco Ayala, et al., "Cognitive Impairment Induced by Lead Exposure during Lifespan: Mechanisms of Lead Neurotoxicity," *Toxics* 9, no. 2 (2021): 23.

4. A. G.-M. Ferrari, P. Carrington, S. J. Rowley-Neale, and C. E. Banks, "Recent Advances in Portable Heavy Metal Electrochemical Sensing Platforms," *Environmental Science: Water Research & Technology* 6, no. 10 (2020): 2676–2690.

5. C. Ariño, C. E. Banks, A. Bobrowski, et al., "Electrochemical Stripping Analysis," *Nature Reviews Methods Primers* 2, no. 1 (2022): 62.

6. J. Wang, "Stripping Analysis at Bismuth Electrodes: A Review," *Electroanalysis* 17, no. 15-16 (2005): 1341–1346, https://doi.org/10.1002/elan.200403270.

7. (a) C. A. de Lima and A. Spinelli, "Electrochemical Behavior of Progesterone at an Ex Situ Bismuth Film Electrode," *Electrochimica Acta* 107 (2013): 542–548. (b) S. B. Hočevar, S. Daniele, C. Bragato, and B. Ogorevc, "Reactivity at the Film/Solution Interface of Ex Situ Prepared Bismuth Film Electrodes: A Scanning Electrochemical Microscopy (SECM) and Atomic Force Microscopy (AFM) Investigation," *Electrochimica Acta* 53, no. 2 (2007): 555–560. (c) E. A. Hutton, S. B. Hočevar, and B. Ogorevc, "Ex Situ Preparation of Bismuth Film Microelectrode for use in Electrochemical Stripping Microanalysis," *Analytica Chimica Acta* 537, no. 1-2 (2005): 285–292.

8. (a) L. Baldrianova, I. Svancara, M. Vlcek, A. Economou, and S. Sotiropoulos, "Effect of Bi (III) Concentration on the Stripping Voltammetric Response of in Situ Bismuth-Coated Carbon Paste and Gold Electrodes," *Electrochimica Acta* 52, no. 2 (2006): 481–490. (b) M. Finšgar and L. Kovačec, "Copper-Bismuth-Film in Situ Electrodes for Heavy Metal Detection," *Microchemical Journal* 154 (2020): 104635. (c) R. Pauliukaitė, S. B. Hočevar, B. Ogorevc, and J. Wang, "*Characterization and Applications of a Bismuth Bulk Electrode. Electroanalysis: An International Journal Devoted to Fundamental and Practical Aspects of Electroanalysis,*" 16, no. 9 (2004): 719–723.

9. R. O. Kadara, N. Jenkinson, and C. E. Banks, "Disposable Bismuth Oxide Screen Printed Electrodes for the High Throughput Screening of Heavy Metals," *Electroanalysis* 21, no. 22 (2009): 2410–2414, https://doi.org/10.1002/elan.200900266.

10. R. O. Kadara and I. E. Tothill, "Development of Disposable Bulk-Modified Screen-Printed Electrode Based on Bismuth Oxide for Stripping Chronopotentiometric Analysis of Lead (II) and Cadmium (II) in Soil and Water Samples," *Analytica Chimica Acta* 623, no. 1 (2008): 76–81.

11. N. Lezi, A. Economou, P. A. Dimovasilis, P. N. Trikalitis, and M. I. Prodromidis, "Disposable Screen-Printed Sensors Modified with Bismuth Precursor Compounds for the Rapid Voltammetric Screening of Trace Pb (II) and Cd (II)," *Analytica Chimica Acta* 728 (2012): 1–8.

12. (a) N. Lezi, C. Kokkinos, A. Economou, and M. I. Prodromidis, "Voltammetric Determination of Trace Tl (I) at Disposable Screen-Printed Electrodes Modified with Bismuth Precursor Compounds," *Sensors and Actuators B: Chemical* 182 (2013): 718–724. (b) M. A. Tapia, C. Perez-Rafols, R. Gusmao, N. Serrano, Z. Sofer, and J. M. Díaz-Cruz, "Enhanced Voltammetric Determination of Metal Ions by Using a Bismuthene-Modified Screen-Printed Electrode," *Electrochimica Acta* 362 (2020): 137144.

13. R. D. Crapnell, C. Kalinke, L. R. G. Silva, et al., "Additive Manufacturing Electrochemistry: An Overview of Producing Bespoke Conductive Additive Manufacturing Filaments," *Materials Today* 71 (2023): 73–90, https://doi.org/10.1016/j.mattod.2023.11.002.

14. (a) I. V. Arantes, R. D. Crapnell, E. Bernalte, M. J. Whittingham, T. R. Paixão, and C. E. Banks, "Mixed Graphite/Carbon Black Recycled PLA Conductive Additive Manufacturing Filament for the Electrochemical Detection of Oxalate," *Analytical Chemistry* 95, no. 40 (2023): 15086–15093. (b) K. K. Augusto, R. D. Crapnell, E. Bernalte, et al., "Optimised Graphite/Carbon Black Loading of Recycled PLA for the Production of Low-Cost Conductive Filament and Its Application to the Detection of β-Estradiol in Environmental Samples," *Microchimica Acta* 191, no. 7 (2024): 375. (c) R. D. Crapnell, I. V. Arantes, M. J. Whittingham, et al., "Utilising Bio-Based Plasticiser Castor Oil and Recycled PLA for the Production of Conductive Additive Manufacturing Feedstock and Detection of Bisphenol A," *Green Chemistry* 25, no. 14 (2023): 5591–5600. (d) R. D. Crapnell and C. E. Banks, "Graphene Additive Manufacturing," in The Handbook of Graphene Electrochemistry, (New York, NY: Springer, 2024), 179–191.

15. R. D. Crapnell, I. V. Arantes, J. R. Camargo, et al., "Multi-Walled Carbon Nanotubes/Carbon Black/rPLA for High-Performance Conductive Additive Manufacturing Filament and the Simultaneous Detection of Acetaminophen and Phenylephrine," *Microchimica Acta* 191, no. 2 (2024): 96.

16. (a) E. Bernalte, K. K. Augusto, R. D. Crapnell, H. G. Andrews, O. Fatibello-Filho, and C. E. Banks, "Eco-Friendly Integration of Gold Nanoparticles into Additive Manufacturing Filaments: Advancing Conductivity and Electrochemical Performance," *RSC Applied Interfaces* (2025), https://doi.org/10.1039/D4LF00368C. (b) C. Kalinke, R. D. Crapnell, E. Sigley, et al., "Recycled Additive Manufacturing Feedstocks with Carboxylated Multi-Walled Carbon Nanotubes toward the Detection of Yellow Fever Virus cDNA," *Chemical Engineering Journal* 467 (2023): 143513.

17. E. Koukouviti, A. Economou, and C. Kokkinos, "3D Printable Multifunctional Electrochemical Nano-Doped Biofilament," *Advanced*

18. R. D. Crapnell, I. V. S. Arantes, M. J. Whittingham, et al., "Utilising Bio-Based Plasticiser Castor Oil and Recycled PLA for the Production of Conductive Additive Manufacturing Feedstock and Detection of Bisphenol A," *Green Chemistry* 5591–5600, 25 (2023): https://doi.org/10.1039/D3GC01700A.

19. E. Bernalte, R. D. Crapnell, O. M. Messai, and C. E. Banks, The Effect of Slicer Infill Pattern on the Electrochemical Performance of Additively Manufactured Electrodes," *ChemElectroChem* (2024): e202300576.

20. R. D. Crapnell, A. Garcia-Miranda Ferrari, M. J. Whittingham, et al., "Adjusting the Connection Length of Additively Manufactured Electrodes Changes the Electrochemical and Electroanalytical Performance," *Sensors* 22, no. 23 (2022): 9521.

21. R. Blume, D. Rosenthal, J. P. Tessonnier, H. Li, A. Knop-Gericke, and R. Schlögl, "Characterizing Graphitic Carbon with X-Ray Photoelectron Spectroscopy: A Step-by-Step Approach," *ChemCatChem* 7, no. 18 (2015): 2871–2881.

22. (a) M. Jiang, Y. Ding, H. Zhang, et al., "A Novel Ultrathin Single-Crystalline Bi2O3 Nanosheet Wrapped by Reduced Graphene Oxide with Improved Electron Transfer for Li Storage," *Journal of Solid State Electrochemistry* 24, no. 10 (2020): 2487–2497, https://doi.org/10.1007/s10008-020-04788-8. (b) N. A. Kouamé, O. T. Alaoui, A. Herissan, et al., "Visible Light-Induced Photocatalytic Activity of Modified Titanium(iv) Oxide with Zero-Valent Bismuth Clusters," *New Journal of Chemistry* 39, no. 3 (2015): 2316–2322, https://doi.org/10.1039/C4NJ01979B.

23. F. Arduini, J. Q. Calvo, G. Palleschi, D. Moscone, and A. Amine, "Bismuth-Modified Electrodes for Lead Detection," *TrAC Trends in Analytical Chemistry* 29, no. 11 (2010): 1295–1304, https://doi.org/10.1016/j.trac.2010.08.003.

24. E. C. Okpara, S. C. Nde, O. E. Fayemi, and E. E. Ebenso, "Electrochemical Characterization and Detection of Lead in Water Using SPCE Modified with BiONPs/PANI," *Nanomaterials* 11, no. 5 (2021): 1294.

25. (a) A. Shah, A. Zahid, A. Khan, et al., "Development of a Highly Sensitive Electrochemical Sensing Platform for the Trace Level Detection of Lead Ions," *Journal of the Electrochemical Society* 166, no. 9 (2019): B3136. (b) E. C. Okpara, O. E. Fayemi, E.-S. M. Sherif, P. S. Ganesh, B. K. Swamy, and E. E. Ebenso, "Electrochemical Evaluation of Cd2+ and Hg2+ Ions in Water Using ZnO/Cu2ONPs/PANI Modified SPCE Electrode," *Sensing and Bio-Sensing Research* 35 (2022): 100476.

26. I. Albalawi, A. Hogan, H. Alatawi, and E. Moore, "A Sensitive Electrochemical Analysis for Cadmium and Lead Based on Nafion-Bismuth Film in a Water Sample," *Sensing and Bio-Sensing Research* 34 (2021): 100454, https://doi.org/10.1016/j.sbsr.2021.100454.

27. G.-H. Hwang, W.-K. Han, J.-S. Park, and S.-G. Kang, "An Electrochemical Sensor Based on the Reduction of Screen-Printed Bismuth Oxide for the Determination of Trace Lead and Cadmium," *Sensors and Actuators B: Chemical* 135, no. 1 (2008): 309–316, https://doi.org/10.1016/j.snb.2008.08.039.

28. M. Mertiri, J. Hrbac, M. Prodromidis, A. Economou, and C. Kokkinos, "Digital Fabrication of 3D Printed Bismuth Sparked Sensors for Electrochemical Sensing," *Applied Materials Today* 39 (2024): 102289, https://doi.org/10.1016/j.apmt.2024.102289.

29. R. O. Kadara, N. Jenkinson, and C. E. Banks, "Disposable Bismuth Oxide Screen Printed Electrodes for the High Throughput Screening of Heavy Metals," *Electroanalysis* 21, no. 22 (2009): 2410–2414.

30. (a) R. O. Kadara and I. E. Tothill, "Resolving the Copper Interference Effect on the Stripping Chronopotentiometric Response of Lead (II) Obtained at Bismuth Film Screen-Printed Electrode," *Talanta* 66, no. 5 (2005): 1089–1093. (b) M. Finšgar and K. Jezernik, "The Use of Factorial Design and Simplex Optimization to Improve

Analytical Performance of In Situ Film Electrodes," *Sensors* 20, no. 14 (2020): 3921.

31. X. Xuan and J. Y. Park, "A Miniaturized and Flexible Cadmium and Lead Ion Detection Sensor Based on Micro-Patterned Reduced Graphene Oxide/Carbon Nanotube/Bismuth Composite Electrodes," *Sensors and Actuators B: Chemical* 255 (2018): 1220–1227.

32. J. Wang, J. Lu, Ü.A. Kirgöz, S. B. Hocevar, and B. Ogorevc, "Insights into the Anodic Stripping Voltammetric Behavior of Bismuth Film Electrodes," *Analytica Chimica Acta* 434, no. 1 (2001): 29–34.

Supporting Information

Additional supporting information can be found online in the Supporting Information section.